Materials Advances

ROYAL SOCIETY OF CHEMISTRY

PAPER

View Article Online
View Journal | View Issue

Cite this: *Mater. Adv.*, 2025, 6, 5576

Unveiling the impact of synthesis routes on water and ethanol sorption performance of ZIF-71 and ZIF-93†

Ciara Byrne, *[ab] Katja Vodlan, [ac] Connor Hewson,[d] Paul Iacomi, [d] Amalija Golobič[c] and Nataša Zabukovec Logar [ab]

Interest in the large-scale applications of metal–organic frameworks (MOFs) has grown in the last 10 years. However, applying MOFs in real life situations remains challenging due to the high cost associated with mass production and their potential negative effects on the environment. In this study, ZIF-71 and ZIF-93 frameworks were synthesized at room temperature using greener solvents (water, methanol, and ethanol) and *via* mechanochemical synthesis. Structural and textural analyses revealed that the structural and textural properties of the ZIFs were mostly preserved, with the mechanochemically prepared samples exhibiting slightly reduced crystallinity and microporosity compared to those prepared using established solvothermal synthesis methods. The water and ethanol sorption performance study of the samples revealed comparable water and ethanol uptake for the entire ZIF-93 series and for the sample prepared by methods from the literature. The same applies to the ZIF-71 series, except for one ZIF-71 sample synthesized using the liquid-assisted ball milling method, which showed reduced water and ethanol uptake due to partial degradation of the structure during the sorption study. The stability study of the four best-performing samples over up to 20 sorption/desorption cycles revealed that the samples prepared using ball milling and the precipitation method, maintained their initial capacity throughout the evaluated cycling program, suggesting promising long-term performance.

Received 15th April 2025,
Accepted 23rd June 2025

DOI: 10.1039/d5ma00367a

rsc.li/materials-advances

Introduction

Sorption-based technologies are widely recognized for their efficiency in various applications, including thermal energy management, gas separation, water harvesting, and environmental remediation.[1–3] These technologies rely on the ability of materials to adsorb and desorb gases or vapours through precise interactions, enabling energy-efficient processes with minimal environmental impact.

Especially relevant in recent research are sorption-based thermochemical energy storage (TCES) and adsorption heat pump (AHP) technologies, which use reversible chemical reactions and/or sorption processes of gases and vapours in solids. One major benefit of using these methods is that they enable an insignificant amount of heat loss while reaching higher energy transformation and storage performance[4,5] with storage densities comparable to those of state-of-the-art Li-ion batteries.[6] TCES and AHP have the capacity to utilize solar thermal energy and low-grade or renewable heat sources to dry and activate the adsorbent material, leading to a significant reduction in CO_2 emissions.

The need to further improve the current performance and efficiency of adsorbents for thermal management at optimal conditions (*e.g.*, for TECS maximising adsorption/desorption within the 0.1 to 0.4 relative pressure range, activating materials at temperatures below 150 °C and cycling stability) explains the continued interest of researchers in this field, and highlights the significant amount of work still required.[7]

Currently, studies are primarily focused on traditional (*e.g.*, zeolites) and innovative (*e.g.*, metal–organic frameworks (MOFs), aluminophosphates and composites) sorbents.[5,8] Generally, the drawback of zeolites is their activation temperature, which is too high to be achieved with conventional solar collectors or other low-grade heat sources. Aluminophosphates fulfil most performance requirements but are expensive to synthesise, and composites from inorganic salts and porous supports generally suffer from salt leaching and subsequent material degradation.[4,9]

[a] *National Institute of Chemistry, 1000 Ljubljana, Slovenia. E-mail: ciara.byrne@ki.si*
[b] *School of Science, University of Nova Gorica, 5000 Nova Gorica, Slovenia*
[c] *Faculty of Chemistry and Chemical Technology, University of Ljubljana, 1000 Ljubljana, Slovenia*
Surface Measurement Systems Ltd, Unit 5 Wharfside, London, HA0 4PE, UK

† Electronic supplementary information (ESI) available. See DOI: https://doi.org/10.1039/d5ma00367a

MOFs, crystalline porous materials, are formed from metal ions or clusters (Zn, Cr, Cu, Ni, *etc.*) bridged by organic ligands,[10,11] such as carboxylates.[12] Zeolitic imidazolate frameworks (ZIFs) are a subclass of MOFs, with imidazolate linkers and zeolite-like topologies.[13,14] Due to the strong bonds between the cation of the metallic centres and nitrogen of the imidazole anion, ZIFs are considered to be thermochemically more stable when compared to other MOFs. In addition to their large specific surface areas and porosity, ZIFs can contain various functional groups on the imidazolate ligand and exhibit pore sizes above 1 nm, which makes them potentially suitable sorbents for sorption-based thermal management.[15]

In recently reported studies, different types of working fluids/adsorbates have been tested. However, water is the most frequently used adsorbate, as it is environmentally friendly.[9,13,16–18] The capacity and mechanism of water adsorption, which determine the performance of thermal batteries and heat pumps, depend on the hydrophilicity/hydrophobicity of the functional groups, the pore size and the geometry/topology of the frameworks. Gao *et al.* investigated the adsorption behaviour of water for 7 different ZIFs.[17] The study revealed that ZIFs with non-polar groups, such as ZIF-8, have weak interactions with water, leading to hydrophobicity and low uptakes. Conversely, ZIFs with polar groups, such as ZIF-93 and SIM-1/ZIF-94, form hydrogen bonds with water, which promotes its adsorption. It was also reported that ZIF-93 has a higher porosity, lower density and significantly higher water adsorption at high relative pressures than SIM-1/ZIF-94 with the same molecular formula but different topology.[17,19]

To further explore the potential of hydrophobic ZIFs, other alternatives for working fluids were suggested, like methanol and ethanol.[13,15,20–22] Lange *et al.* examined the benefits of switching water for ethanol as a working fluid in adsorption-driven heat pumps and chillers for 18 MOFs and reported on the more efficient use of larger pores, occurrence of adsorption at lower partial pressures, lesser impact of polar/apolar functionalities in MOFs, and improved stability. Additionally, the freezing point of ethanol is lower than water, so it can be used in cooler environments.[21] In our recent study, we studied seven different ZIFs (ZIF-8, ZIF-62, ZIF-71, ZIF-74, ZIF-76, ZIF-90 and ZIF-93) and their heat storage potential using water and ethanol as working fluids.[15] It was demonstrated that the storage performance is governed by several factors, including the pore dimensions, type and distribution of functional groups on imidazolate ligands, chemical stability of the framework, as well as the type of working fluid. Ethanol sorption data demonstrated inflection points in the sorption isotherms at lower relative pressures, and enhancement of uptakes for ZIFs with hydrophobic properties, but lower desorption enthalpies when compared to water sorption. We found that ZIF-93 was the most promising material for both working fluids.

In spite of the demonstrated potential of ZIFs for many different applications, their large-scale application is still limited by the absence of low-cost mass production, as well as the lack of sustainable synthesis routes that would lower the environmental impact of the ZIF preparation.[23,24] Traditionally, most of the stable ZIFs are synthesized *via* solvothermal synthesis, which requires higher temperatures, can take up to 72 h or more and/or need to be activated.[11,13,15,17,24–30] Additionally, large quantities of a polar aprotic solvent *N*,*N*-dimethylformamide (DMF) are often used as well. This is due to its ability to dissolve a wide range of metal salts and organic linkers, and its ability to act as a catalyst for the reaction.[11,13,15,17,24–30] Since DMF is known to be toxic and carcinogenic, much attention has been focused on implementing greener solvents to the ZIF synthesis process and lowering its impact on the environment.[25] For example, DMF was successfully replaced with methanol in the synthesis of ZIF-71 and ZIF-93.[17,20,31,32] Furthermore, Ramos-Fernandez *et al.* synthesized ZIF-93 by water-based room temperature synthesis.[33] Alternative organic solvents, such as dihydrolevoglucosenone (commercial name Cyrene™), gamma-valerolactone (GVL), dimethyl sulfoxide (DMSO), TamiSolve® and methyl 5-(dimethylamino)-2-methyl-oxo-pentanoate, were also used for the synthesis of different ZIFs.[25] Despite the great progress that has been made toward achieving a greener solvothermal synthesis of ZIFs and other MOFs, the addition of reaction modulators (such as triethylamine, ammonia, formic acid, hydrochloric acid, *etc.*) is necessary to reduce the reaction temperature and shorten the synthesis time, which again leads to higher cost and possible environmental pollution.[24,34–40] In recent years, many alternative synthesis techniques (mechanochemical, microwave-assisted, sonochemical) have been examined to reduce the reaction time and the quantity of solvents used. Among them, mechanochemical synthesis is the most promising, as no (neat grinding) solvent or only a minimal amount of solvent (liquid-assisted grinding) is needed. Furthermore, the reaction proceeds without extra heating and takes less than an hour to complete.[12,41] In the last couple of years, the mechanochemical syntheses of ZIF-8, ZIF-62 and ZIF-67 have been reported.[42–46] For the synthesis of ZIFs, liquid-assisted grinding is most commonly used. The small amount of auxiliary solvent (50 to 400 μL) increases the speed of synthesis and yield, but it can affect the topology of the framework as well.[41]

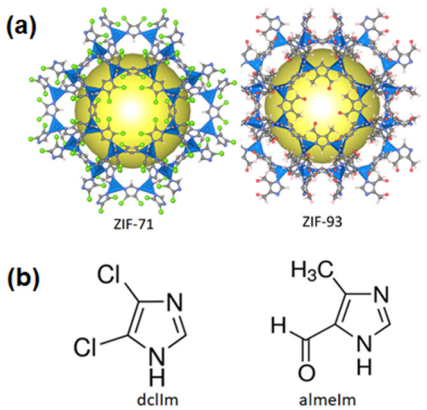

Fig. 1 (a) RHO topology of ZIF-93 and ZIF-71. ZnN_4 tetrahedra are shown in blue, and the yellow spheres indicate empty spaces in the cage. Linkers are shown in ball and stick representation (H in pink, C in grey, N in blue, O in red and Cl in green). (b) The structure of 4,5-dichloroimidazole (dcIIm) and 4-methyl-5-imidazolecarboxaldehyde (almeIm), which are the linkers for ZIF-71 and ZIF-93, respectively.

Table 1 Pore entrance size (d_a^g), the pore/cage capacity (d_p^h) and topology for the two examined ZIFs

ZIF	d_a^g [Å]	d_p^h [Å]	Topology	Ref.
ZIF-71	4.2	16.5	RHO	27 and 48
ZIF-93	3.6	17.9	RHO	47

In this work, ZIF-93 and ZIF-71 with the same RHO topology and similar pore sizes were studied (Fig. 1(a) and Table 1) under conditions suitable for sorption-based TCES application with water and ethanol as working fluids.[6,27,47] ZIF-71 contains the hydrophobic 4,5-dichloroimidazole ligand, while ZIF-93 uses the polar 4-methyl-5-imidazolecarboxaldehyde ligand, which makes it hydrophilic (Fig. 1(b)). The aim of the study was to better understand the influence of the synthesis conditions on the sorption performance of both solvothermally and mechanochemically prepared ZIFs. The mechanochemical preparation was introduced as a step toward achieving a more sustainable synthesis of the selected materials and possible mass production for large-scale applications. Furthermore, the emphasis was on the study of the materials' hydrothermal stability, which is of utmost importance for water-based sorption applications.

Experimental

An extensive and systematic study on the synthesis of ZIF-71 and ZIF-93 *via* solvothermal, precipitation and mechanochemical methods was completed. The main body of this manuscript will only discuss the samples that showed the most notable results. A detailed list of the synthesis conditions for the samples that will not be discussed can be found in the ESI† in Tables S1–S6.

Materials

Zinc acetate dihydrate ($Zn(OAc)_2{\cdot}2H_2O$, 98%), zinc nitrate hexahydrate ($Zn(NO_3)_2{\cdot}6H_2O$, 99%), zinc oxide (ZnO, 99%), ammonium chloride (NH_4Cl, 99.5%), formic acid (HCOOH, 95%) and γ-valerolactone (GVL, 99%) were purchased from Sigma Aldrich (Darmstadt, Germany). 4,5-Dichloroimidazole (dclIm, 99%) was purchased from Abcr (Karlsruhe, Germany). 4-Methyl-5-imidazolecarboxaldehyde (almeIm, 99%) was purchased from Fluorochem (Hadfield, UK). Methanol (CH_3OH, 99.9%) and *N*,*N*-dimethylformamide (DMF, 99.8%) were purchased from Honeywell Fluka (Seelze, Germany). Acetic acid (CH_3COOH, 99.8%) was purchased from Carlo Erba (Val de Reuil, France). GVL was mixed with MeOH in a 1 : 1 ratio prior to use. This mixture will be denoted as 'GVL' in the synthesis methods. All remaining chemicals were used without any further treatment.

Solvothermal & precipitation synthesis of ZIF-93

1-ZIF93-ST was synthesised according to our previous study and used for comparison purposes.[15] The synthesis of ZIF-93 used a 1 : 3 : 371 molar ratio for zinc acetate dihydrate, 4-methyl-5-imidazolecarboxaldehyde and methanol. The reaction conditions are presented in Table 2. The remaining samples were synthesised based on the modified method published by Ramos-Fernandez *et al.*[33] For all 4 samples, the same molar ratio of 1 Zn : 2 almeIm : 1 NH_3 : 135 H_2O was used. In a glass beaker, a mixture of zinc salt and linker was prepared by adding 1.05 g of $Zn(NO_3)_2{\cdot}6H_2O$ or 0.78 g of $Zn(OAc)_2{\cdot}2H_2O$ and 0.88 g of almeIm to 56 mL of deionized water. The mixture was stirred until both powdered reactants had fully dissolved. In a separate beaker, 480 μL of 30% ammonia solution was added to 40 mL of deionized water. The solution was stirred and later added dropwise to the solution of zinc salt and linker. After stirring for 4–18 h at room temperature (RT), the resulting mixture was centrifuged at 3500 rpm for 15 min. The precipitate was washed with water and centrifuged again. After repeating the same process, the sample was left to dry at room temperature overnight and activated for 18 h in a vacuum oven at 150 °C. More information on the synthesis conditions is provided in Table 2.

Table 2 Reaction conditions for the studied ZIF-71 and ZIF-93 samples, where RT denotes room temperature and N/A indicates non-applicable

Sample	Zinc precursor	Solvent	Time	Temp.
1-ZIF71-P	$Zn(NO_3)_2{\cdot}6H_2O$	MeOH	18 h	RT
2-ZIF71-P	$Zn(OAc)_2{\cdot}2H_2O$	MeOH	1 h	RT
3-ZIF71-P	$Zn(OAc)_2{\cdot}2H_2O$	EtOH	1 h	RT
4-ZIF71-BM	$ZnO/Zn(OAc)_2{\cdot}2H_2O$	GVL	45 min	N/A
5-ZIF71-BM	$ZnO/Zn(OAc)_2{\cdot}2H_2O$	N/A	17 min	N/A
1-ZIF93-ST	$Zn(OAc)_2{\cdot}2H_2O$	MeOH	24 h	85 °C
2-ZIF93-P	$Zn(NO_3)_2{\cdot}6H_2O$	H_2O	18 h	RT
3-ZIF93-P	$Zn(OAc)_2{\cdot}2H_2O$	H_2O	4 h	RT
4-ZIF93-P	$Zn(OAc)_2{\cdot}2H_2O$	H_2O	5 h	RT
5-ZIF93-BM	$ZnO/Zn(OAc)_2{\cdot}2H_2O$	H_2O	45 min	N/A
6-ZIF93-BM	$ZnO/Zn(OAc)_2{\cdot}2H_2O$	H_2O/GVL	30 min	N/A

Mechanochemical synthesis of ZIF-93

For 5-ZIF93-BM, 0.07 g ZnO (0.9 mmol) and 0.02 g $Zn(OAc)_2{\cdot}2H_2O$ (0.1 mmol) were ground with an agate mortar and pestle. The ground reactants were added to a 10 mL ball mill grinding jar along with 0.22 g (2 mmol) almeIm linker, 45 μL (2.5 mmol) deionized water, 5 μL 30% (0.01 mmol) NH_3 solution and 2 stainless steel grinding balls with a diameter of 10 mm. The reaction mixture was milled with the Retsch Mixer Mill MM 400 for 45 min at a frequency of 30 Hz. For 6-ZIF93-BM, 0.0653 g ZnO (0.9 mmol) and 0.0439 g $Zn(OAc)_2{\cdot}2H_2O$ (0.1 mmol) were ground with an agate mortar and pestle. The ground reactants were added to a 10 mL ball mill grinding jar along with 0.2202 g (2 mmol) almeIm linker, 100 μL (11.1 mmol) deionized water, 100 μL (2 mmol) GVL and 2 stainless steel grinding balls with a diameter of 10 mm. The reaction mixture was milled with the Retsch Mixer Mill MM 400 for 30 min at a frequency of 30 Hz. The resulting powders were suspended in EtOH and centrifuged for 7 min at 5500 rpm. The precipitates were dried overnight in a convection oven at 60 °C. The dried samples were then activated in a vacuum oven at 120 °C overnight.

Precipitation synthesis of ZIF-71

As with ZIF-93, the synthesis method from our previous study was used for comparison purposes, and the reaction conditions can be seen in Table 2.[15] This sample was denoted as 1-ZIF71-P

and had a reaction ratio of 0.66 mmol : 3.14 mmol : 1.48 mol for zinc nitrate hexahydrate, dichloroimidazole and methanol, respectively.[15] 2-ZIF71-P was synthesized using a modified method from Yuan *et al.*[32] In a glass beaker, 0.22 g (1 mmol) $Zn(OAc)_2{\cdot}2H_2O$ was dissolved in 10 mL (247 mmol) MeOH (Solution A). A ligand solution was prepared by stirring the mixture of 0.55 g (4 mmol) dclIm, 10 mL (247 mmol) MeOH and 38 μL (1 mmol) HCOOH (Solution B). Solution B was added dropwise to solution A. The mixture was covered and stirred at room temperature for 1 h. The mixture was then centrifuged for 8 min at 5500 rpm. The obtained product was dried at room temperature overnight. For the synthesis of 3-ZIF71-P, the method was modified by substituting 10 mL of MeOH with 8 mL of EtOH in the preparation step of both solutions.

Mechanochemical synthesis of ZIF-71

For 4-ZIF71-BM, 0.07 g ZnO (0.9 mmol) and 0.02 g $Zn(OAc)_2{\cdot}2H_2O$ (0.1 mmol) were ground with an agate mortar and pestle, and transferred to the 10 mL ball mill grinding jar. After the addition of 0.28 g (2 mmol) dclIm linker, 45 μL (0.47 mmol) GVL, 5 μL 30% (0.1 mmol) NH_3 solution and 2 stainless steel grinding balls with a diameter of 10 mm to the jar, the reaction mixture was milled with the Retsch Mixer Mill MM 400 at a frequency of 45 Hz for 30 min. For 5-ZIF71-BM, 0.1303 g ZnO (0.9 mmol), 0.5479 g (3.9 mmol) dclIm linker and 0.0880 g $Zn(OAc)_2{\cdot}2H_2O$ (0.1 mmol) were added to the 25 mL ball mill grinding jar. Then, 2 stainless steel grinding balls with a diameter of 15 mm were added to the jar, and the reaction mixture was milled with the Retsch Mixer Mill MM 400 at a frequency of 20 Hz for 17 min. The obtained powders were suspended in EtOH and centrifuged for 6 min at 4500 rpm. The products were dried in a convection oven at 60 °C overnight. These samples were activated by soaking in MeOH, and then outgassed in a vacuum oven at 150 °C overnight.

Characterisation methods

The PXRD patterns of the as-synthesized and activated samples were recorded using a PANalytical X'Pert PRO diffractometer with a fully opened 100 channel X'Celerator detector Plus. Cu-K_α radiation with a wavelength λ = 1.5418 Å was used. The produced PXRD patterns were examined in the 2θ range of 5–50° with a step size of 0.034° per 100 s. The PXRD patterns were analysed using the HighScore Plus 4.9 program.

TGA of the as-synthesized and activated samples was performed on a TA Instruments Q5000 to determine the stability of the ZIFs, as well as the % of adsorbed water/ethanol. The analyses were carried out in airflow (25 mL min^{-1} air and 10 mL min^{-1} Ar). Thermal stability was determined in the temperature range of 25–750 °C for ZIF-93 and 25–800 °C for the ZIF-71 samples, both at a ramp rate of 10 °C min^{-1}.

In order to determine the specific surface area, pore volume and pore size distribution of the samples, nitrogen physisorption was conducted. The samples were degassed for 10 h at 150 °C. Nitrogen physisorption isotherms were recorded by using a Quantachrome AUTOSORB iQ3 at −196 °C. The specific surface area, micro pore volume and total pore volume were calculated using the Quantachrome AUTOSORB iQ3 software. The Brunauer–Emmett–Teller (BET) specific surface area was calculated from the adsorption data in the relative pressure range from 0.005 to 0.02. The total pore volume (V_{total}) was calculated from the amount of N_2 adsorbed at P/P_0 = 0.97 and micropore volume (V_{micro}) from the *t*-plot (P/P_0 = 0.15–0.3).

SEM images were taken with a Zeiss Supra 35 VP microscope with an aperture size of 30 μm and an electron high-tension voltage of 1.00 kV.

Single component vapour isotherms and cycling measurements were performed in a DVS Vacuum gravimetric sorption analyser from Surface Measurement Systems. In this setup, a continuous adsorbate flow enters the sample enclosure, passes a suspended sample pan, and is entrained by a vacuum system. The total pressure is maintained by a backpressure regulating valve located before the outlet. The analyte is sourced from the headspace of a temperature-controlled reservoir. Uptake is measured by a microbalance capable of measuring mass changes at a resolution of 0.01 mg. The entire sample enclosure is kept in a temperature-controlled chamber to avoid any condensation points. For each experiment, between 6 and 20 mg of as-synthesised fresh sample was loaded in the sample holder. The sample was outgassed *in situ* to a pressure of approximately 10^{-6} Torr under a secondary vacuum at 150 °C for 600 minutes. Pure vapour was flowed continuously over the sample at a controlled rate of 5 sccm. Kinetic data were recorded with a resolution of 1 Hz, and the mass stability was used to determine the equilibration by automatically monitoring the rate of change (dm/dt) until it was below 0.006% min^{-1} for at least 10 minutes. Carrier vapour isotherms were performed in a DVS Endeavour from Surface Measurement Systems. This device is a high throughput 5x gravimetric sorption analyser that uses a partially vapour-saturated carrier gas at ambient pressure as the test gas, in this case nitrogen. Outgassing conditions were identical as in the pure vapour experiments except carried out under 100 sccm flow of nitrogen. The sample mass requirements, recording resolution and equilibrium criteria were identical to the pure vapour experiments.

Results and discussion

Structural and physicochemical properties of the synthesized ZIFs

The structural properties of the synthesized materials were examined using PXRD, TGA, N_2 physisorption and SEM. The PXRD analysis shows that ZIF-93 structures were formed in all 6 samples (Fig. 2) and the structure remained intact after the activation process (Fig. S1, ESI†). The same was confirmed for the ZIF-71 samples (Fig. 2 and Fig. S1, ESI†). Additional crystalline phases were confirmed in the samples. However, traces of ZnO are possible in BM samples as residual unreacted ZnO. The presence of a diffraction maximum at 5.6° 2θ in the XRD pattern of the as-synthesised 2-ZIF93-P sample, but not in its activated form, might be due to a long-range arrangement of extra-framework molecules in the as-synthesised sample, which

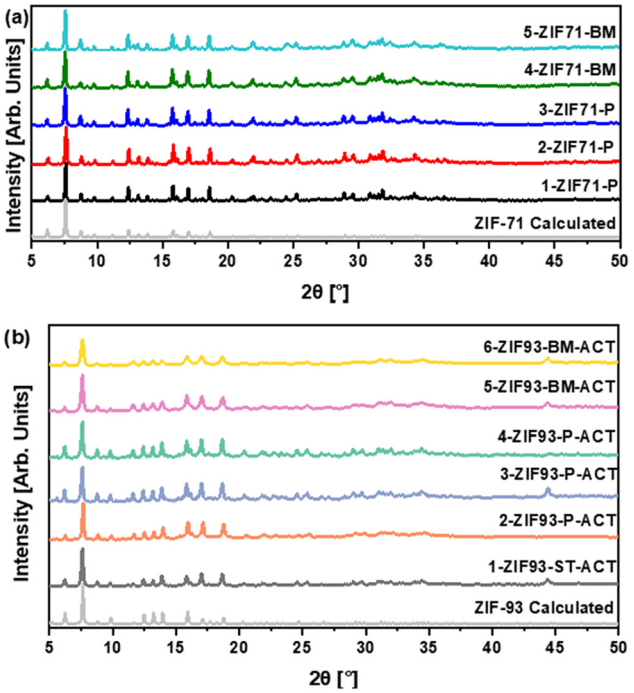

Fig. 2 PXRD patterns of the as-synthesised (a) ZIF-71 and (b) ZIF-93 samples compared to their respective calculated patterns.

are removed with activation or in the presence of some impurity, which again is removed under the activation conditions.

The crystallite size was calculated from XRD by using the Scherrer equation. It can be seen from Table S7 (ESI†) that the size of the primary crystallites of ZIF-93, synthesized *via* mechanochemical method, is 1.5 times smaller than the size of the solvothermally synthesized ZIF-93 *via* precipitation method. For the ZIF-71 system, this trend is not observed because the size of all crystallites is the same, except the size of the solvothermally prepared sample. A peak is observed in some of the diffractograms at 44° 2θ, which is attributed to the sample holder. It is important to note that the calculated values from the Scherrer equation need to be considered as an estimation due to the limitations of the validity of the method to particle sizes of up to 100 nm.

TGA analysis was first performed on the as-synthesized samples and later repeated on the activated samples (see Fig. 3 and Fig. S2, S3, ESI†). The weight losses up to 100 °C are negligible for most ZIF-71 samples due to the hydrophobicity of the framework (Fig. 3 and Fig. S2, ESI†). For 5-ZIF71-BM, a small weight loss due to the removal of the solvent from the pores up to 300 °C can also be seen as well, which suggests that the material requires activation (Fig. 3(b)). The weight change after 300 °C was due to the gradual degradation of the framework.

Conversely, the as-synthesised ZIF93 samples all show weight losses of up to 100 °C, which is in accordance with the hydrophilic nature of the material. The most pronounced weight loss between 100 °C and 300 °C attributed to solvent removal is found in the DTG curve of the as-synthesised 6-ZIF93-BM (Fig. 3(d)). The weight change in the samples after 300 °C was due to the gradual degradation of the framework. Furthermore, peaks at around 30 °C are also present after

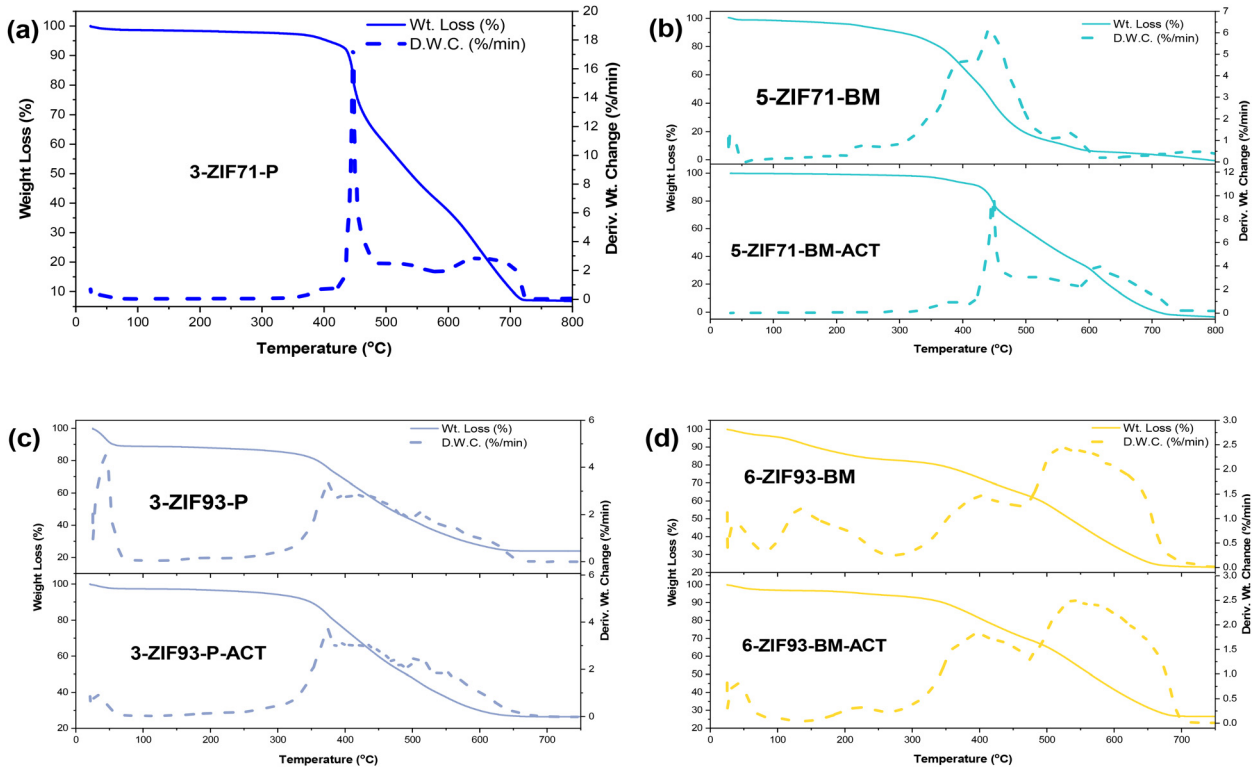

Fig. 3 TGA of the as-synthesised and activated (a) 3-ZIF71-P, (b) 5-ZIF71-BM, (c) 3-ZIF93-P and (d) 6-ZIF93-BM.

activation due to air exposure of the samples before the measurement. The peak between 100 °C and 300 °C disappears after activation in all samples, except for 6-ZIF93-BM (Fig. 3(d)). This is likely due to only partial removal of the GVL from the pores.

All as-synthesized samples were further analysed by SEM imaging (Fig. 4 and 5). Most of the samples appear to have a single phase, with traces of unreacted reagents or carbon coating, which was applied before the analysis. However, the 5-ZIF93-BM sample (Fig. 5(e)) and 6-ZIF93-BM sample (Fig. 5(f)) seem to have two phases. One phase consists of ZIF-93 small particles with diameters of up to 300 nm, which is consistent with the results of the PXRD analysis. Phase 2 is made of larger crystallites with diameters from 1 to 4 μm. We speculate that the sample contains SIM-1/ZIF-94 with sodalite (SOD) topology. However, it cannot be confirmed by PXRD because the peak positions of ZIF-94 almost completely overlap with the positions for ZIF-93.

Based on the calculations with the Scherrer equation (Table S2, ESI†), the primary crystallites in the 1-ZIF93-ST sample, prepared *via* solvothermal synthesis, are nanosized with a diameter of 65 nm. The estimated diameter from the SEM images is 80–100 nm (Fig. 5(a)). There is larger observed discrepancies in the calculated particle size and estimated from SEM for the other samples (*e.g.*, 600 nm to 900 nm for 2-ZIF93-P particles estimated from SEM (Fig. 5(b)) and 90 nm calculated from PXRD). This indicates that the samples consist of polycrystalline or agglomerated particles. It is also important to note that the Scherrer equation takes into account coherent scattering and excludes surface-related domains. Therefore, the calculated values are only considered as tentative. The ZIF-71

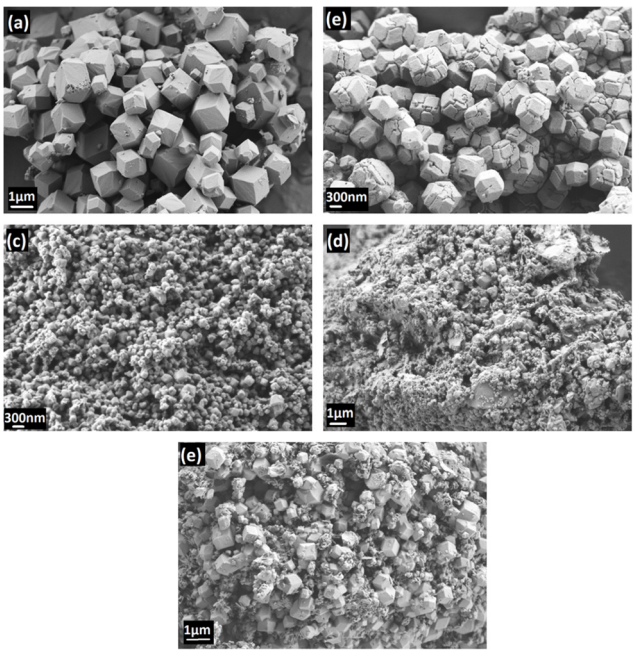

Fig. 4 SEM images of the as-synthesized ZIF-71 showing (a) 1-ZIF71-P, (b) 2-ZIF71-P, (c) 3-ZIF71-P, (d) 4-ZIF71-BM and (e) 5-ZIF71-BM.

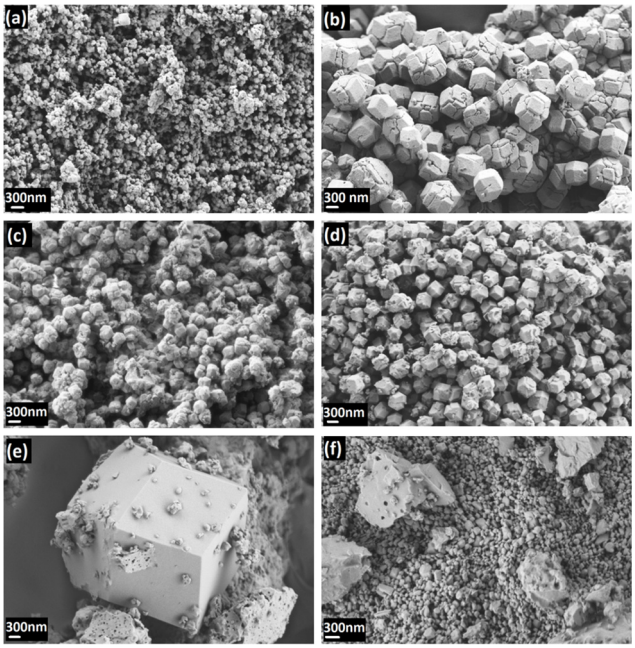

Fig. 5 SEM images of the synthesized ZIF-93 showing (a) 1-ZIF93-ST, (b) 2-ZIF93-P, (c) 3-ZIF93-P, (d) 4-ZIF93-P, (e) 5-ZIF93-BM and (f) 6-ZIF93-BM.

samples are found to be polycrystalline as well: the 2-ZIF71-P and 3-ZIF71-P samples have the narrowest particle size distribution (200–500 nm and 100–300 nm; Fig. 4(b) and (c)). The rest of the samples exhibit sizes from 100 nm to 1 μm.

Calculations based on the Scherrer equation revealed the smallest primary particles in the ball-milled samples (30 nm and 35 nm, respectively).

Nitrogen physisorption was used to determine the pore size distribution and BET specific surface area of the samples. All of the ZIF-93 and ZIF-71 samples present a type 1 isotherm with a small hysteresis loop at relative pressures from 0.9 to 1. In contrast, the 5-ZIF93-BM and 6-ZIF93-BM isotherms exhibit hysteresis loops down to 0.5 relative pressure. The H4 type hysteresis suggests a partial mesoporosity of the samples with the mesopores having access to the surface only *via* small entrances (*e.g.*, slit pores in larger crystallites) (Fig. 6). A small H4 hysteresis was also observed for the 5-ZIF71-BM sample.

Table 3 shows that the 4-ZIF93-P sample with a synthesis time of 5 hours has the highest specific surface area, as well as the highest total pore volume, higher than those of the solvothermally prepared sample 1-ZIF93-ST and precipitation-based sample 3-ZIF93-P (Fig. 6). In the ZIF-71 system, by changing the solvent and the concentration of reactants in the precipitation synthesis of ZIF-71, the total pore volume remains the same, while a decrease in micropore volume and specific surface area can be observed.

Both products synthesized *via* mechanochemical synthesis have lower BET surface area and porosity, compared to the solvothermal products. However, the specific surface areas of both ball mill samples are still in agreement with the results reported in the literature (604–1097 $m^2\ g^{-1}$ for ZIF-93 and 652–1038 $m^2\ g^{-1}$ for ZIF-71), with the BET area of 4-ZIF93-P exceed

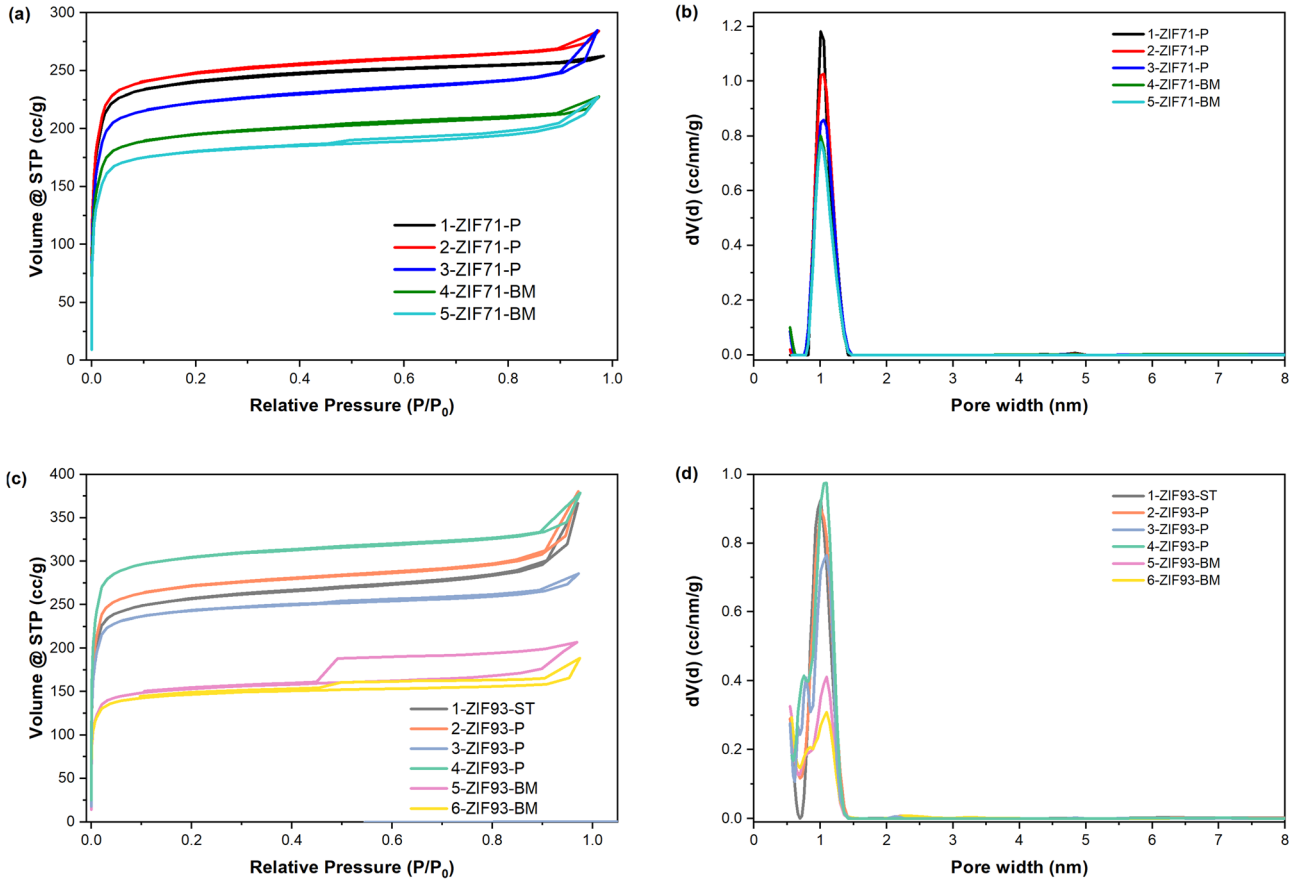

Fig. 6 Nitrogen physisorption isotherms and pore size distributions of the activated (a, b) ZIF-71 and (c, d) ZIF-93 samples.

those values.[15,17,31,33,47,49–52] Again, it has to be taken into the account, that the ball-milled samples are polycrystalline with quite small primary particles and detected mesoporosity. The size of ZIF-93 particles evaluated in the literature was 500–2 mm,[17,33] while the size of the particles in our study was estimated to be in sub-micron region. The exception is ZIF-93 ball-milled samples, where larger particles could belong to SIM-1/ZIF-94 impurities. ZIF-71 crystallite size of less than 100 nm as well as 1 μm[24] was reported in the literature.[31,53] The crystallite size of our ZIF-71 samples was similar ranging from 100–1 μm.

Table 3 Nitrogen physisorption data showing the specific surface area (S_{BET}), micropore volume (V_{micro}) and total pore volume (V_{total}) for all samples

Sample	S_{BET} ($m^2\ g^{-1}$)	V_{micro} ($cm^3\ g^{-1}$)	V_{total} ($cm^3\ g^{-1}$)
1-ZIF93-ST	1030	0.32	0.57
2-ZIF93-P	812	0.25	0.41
3-ZIF93-P	989	0.31	0.44
4-ZIF93-P	1239	0.39	0.59
5-ZIF93-BM	615	0.19	0.32
6-ZIF93-BM	587	0.20	0.29
1-ZIF71-P	981	0.31	0.41
2-ZIF71-P	1008	0.31	0.44
3-ZIF71-P	901	0.28	0.44
4-ZIF71-BM	789	0.25	0.35
5-ZIF71-BM	717	0.25	0.35

Sorption performance studies

As mentioned in the introduction, our previous study showed that 1-ZIF93-ST has the potential for heat storage applications, as it has similar or slightly higher uptake as hydrophilic ZIF-90 but proved to be more stable.[15]

3-ZIF93-P and 2-ZIF71-P were used first to determine the impact using pure vapour and carrier DVS systems (*i.e.*, open or closed systems) had on the total uptake, as it is known that the carrier may have non-negligible uptake.[54] We tested water and ethanol as working fluids. As it can be seen in Fig. S4 (ESI†), there was a slight difference in the water isotherms for 2-ZIF71-P. Otherwise, the water and ethanol isotherms in the different systems showed little to no difference. It is worth noting that while there is next to no difference in the uptakes, there was a difference in the kinetics. Fig. S5 and S6 (ESI†) shows that the kinetics are much faster in a pure vapour system. Therefore, the pure vapour system was used to obtain the isotherms at 25 °C and 35 °C.

Fig. 7 shows all isotherms for all of the ZIF-71 and ZIF-93 samples collected at 25 °C. As it can be seen in Fig. 7(a), the ethanol isotherms for ZIF-71 are S-shaped and the inflection point occurs at low relative pressures ($<0.15\ P/P_0$). The shape of the isotherm indicates a very limited, but noticeable uptake of ethanol at low relative pressure. This is probably due to a partial chemisorption of ethanol on possible surface defect

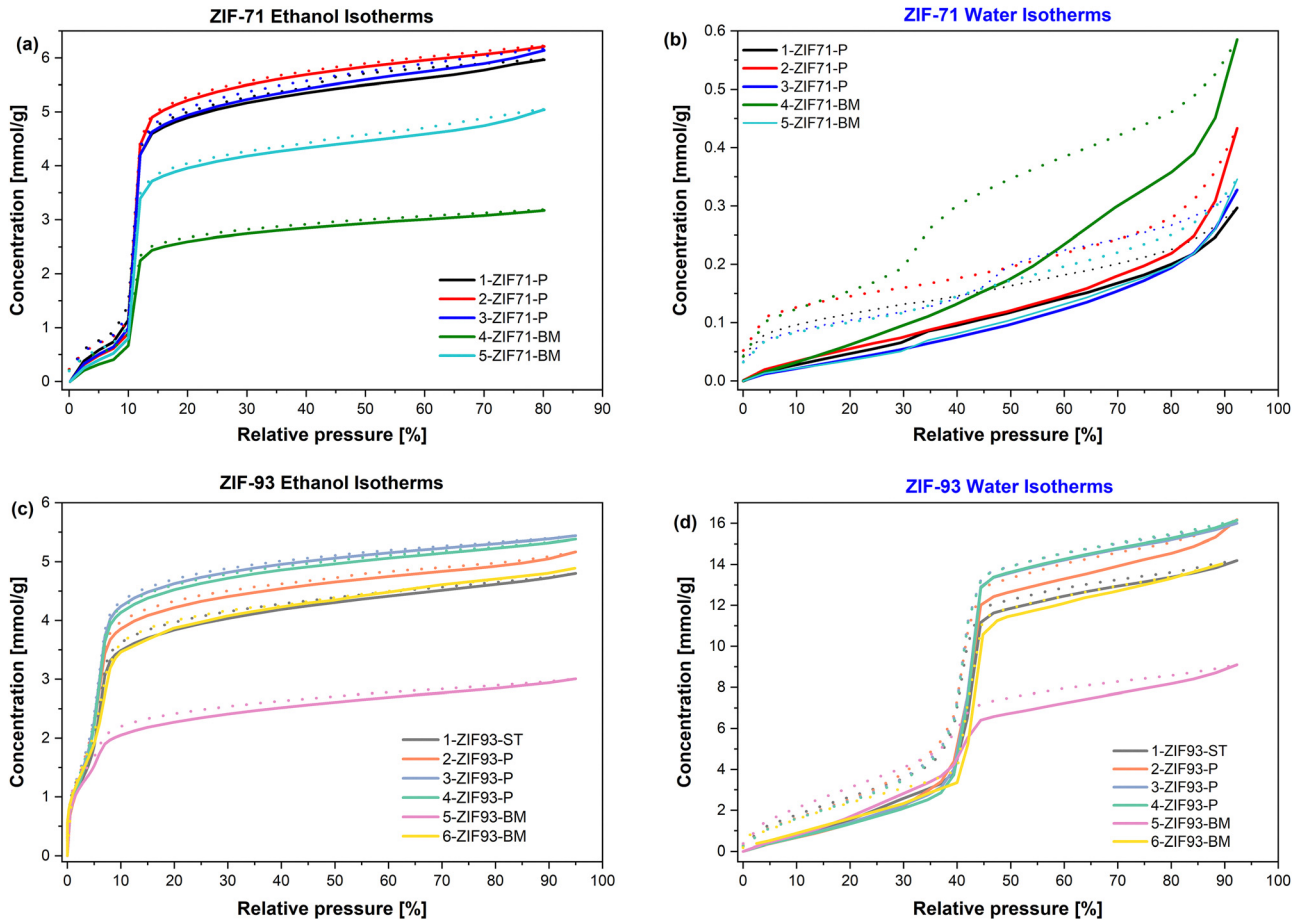

Fig. 7 Ethanol and water isotherms for ZIF-71 (a) and (b) and ZIF-93 (c) and (d) obtained at 25 °C, where the solid lines show the adsorption and the dotted lines shows desorption.

sites, which is followed by a sudden uptake associated with the pore filling phenomenon. There is very little difference between the ethanol uptake at the 'working' relative pressure (0.4 P/P_0) and the maximum relative pressure (0.8 P/P_0), showing only a difference of 0.3–0.7 mmol g^{-1} (Fig. 7, 8 and Fig. S7, ESI†). The ethanol uptake ranges from 5.4-5.7 mmol g^{-1} for the 3 precipitation method samples at 0.4 P/P_0, while the two ball-milled samples had a lower uptake of 2.8 and 4.3 mmol g^{-1} for 4-ZIF71-BM and 5-ZIF71-BM, respectively. When considering the ethanol uptake at the maximum pressure, these figures rise to 5.9–6.2 mmol g^{-1} for the precipitation method samples and 3.2–5.0 mmol g^{-1} for the ball-milled samples. Interestingly, 5-ZIF71-BM (which showed the lower nitrogen physisorption results) proved to be the better performing ball-milled sample. The uptakes for 1-ZIF71-P, 2-ZIF71-P and 3-ZIF71-P are in line with previously published work.[15] At the time of writing, it was not possible to find any sorption studies for ball-milled ZIF-71 samples. As previously mentioned in the introduction and noted in published studies, ZIF-71 is considered to be hydrophobic due to the functional groups from the 4,5-dichloroimidazole linker. Thus, it was expected that the ZIF-71 samples would have a low water uptake. Fig. 7(b) shows that this proved to be the case, with the water uptakes at maximum pressure all being lower than 0.6 mmol g^{-1}.

The results clearly demonstrate that the synthesis method significantly influenced the ZIF-71 ethanol uptakes, *i.e.*, up to 25% lower uptake with the ball-milled samples when compared to the analogues obtained by the precipitation method.

In the ZIF-93 system, the reduction of water and ethanol uptake is up to 15% in the ball-milled samples when compared to the samples obtained by precipitation method. The water and ethanol adsorption isotherms exhibit S-shapes. For water sorption, the inflection point associated with sudden pore filling is at higher relative pressures for all samples (*i.e.*, above 0.4). At lower relative pressures, a small quantity of water is also adsorbed. This is most probably due to surface hydrophilic defects. For ethanol sorption in the ZIF-93 system, the quantity of ethanol adsorbed before the inflection points (ranging from 0.05 to 0.1) is significant, indicating that there is possibly chemisorption also on the carbonyl functional group of ZIF-93.

To simulate adsorption/desorption under application-relevant conditions and to evaluate the long-term stability of the series of materials during use, static isotherms and a series of single-point cycling experiments at 35 °C were performed for the selected precipitation method and ball-milled samples (Fig. 9, 10 and Fig. S7–S9, ESI†). Increasing the acquisition temperature from 25 °C to 35 °C for the water and ethanol

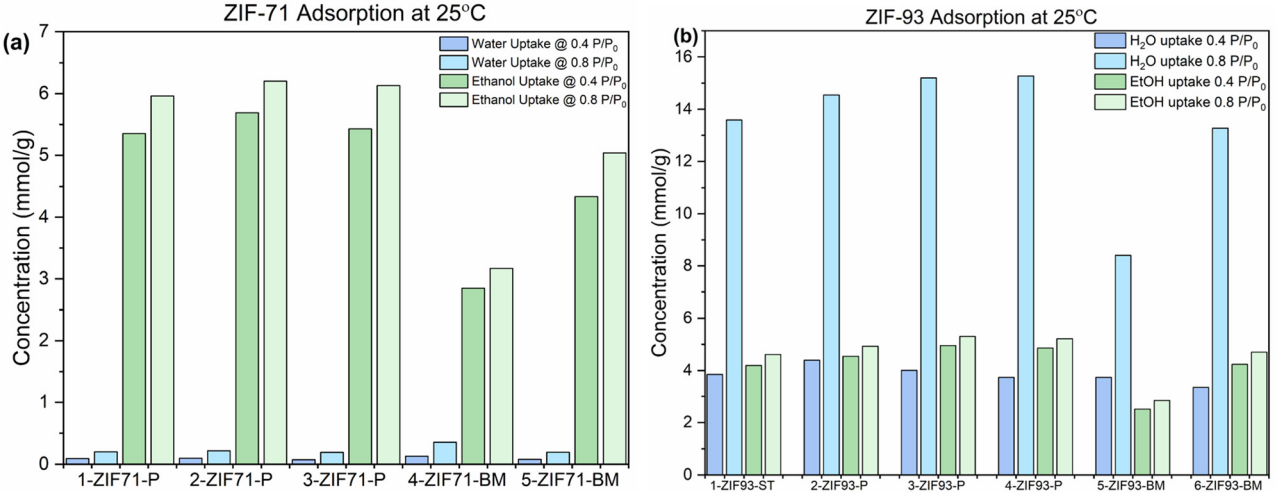

Fig. 8 Bar charts showing the ethanol and water uptake for (a) ZIF-71 and (b) ZIF-93 obtained at 25 °C, showing data for 0.4 P/P_0 and 0.8 P/P_0.

isotherms showed only a maximum of 3% difference in the uptakes (see Fig. 9 and Fig. S7, S8, ESI†). After a preliminary *in situ* high temperature activation (150 °C), the partial pressure of the working fluid was cycled between a fluid loading (heat generation) and a fluid unloading (heat storage) step. The loading point was selected as 0.5 P/P_0 for both water and ethanol, as this point is situated in the isotherm plateau after pore filling is complete, guaranteeing the full use of the material's potential. The unloading point was selected as a mild vacuum (~1–5 Pa). The selected pressures were maintained until the sample mass reached equilibrium. There was no temperature activation between the cycles to best simulate a sequential vacuum-assisted heat pump cycle. Cycles were repeated for at least 5 times for all selected materials (*i.e.*, due to the longer equilibration times for ethanol, 5 cycles were collected, whereas 20 cycles were done for water). The equilibrium uptake at loading for each cycle is shown in Fig. 10 and Fig. S9 (ESI†).

All initial uptakes are fully consistent with the loading obtained in previously measured isotherms.[15] Interestingly, both ZIF-93 samples show the same trend when water is used as a working fluid (Fig. 11(a)) with regards to the uptake and rate of adsorption. A subtle decrease in the maximum loading (<3% of initial capacity) is observed in the first 10 cycles, which may be explained as a partial degradation of the MOF framework. The capacity then stabilizes and remains essentially constant over the remainder of the cycles. When ethanol is the working fluid, the behaviour of the two frameworks is slightly different. Both ZIF-93 samples show a stable capacity over 5 cycles and 20 cycles, respectively. Conversely, the ZIF-71 samples show a subtle decrease in capacity with cycling-evident in 5 cycles and continuing up to 20 cycles. Nevertheless, the capacity loss appears to stabilise and remains below 5% of the initial capacity. The rate of adsorption for ethanol is generally slower than that for water. Furthermore, for both ZIF-71 and ZIF-93 systems, the adsorption desorption cycle is quicker for the ball-milled samples when compared to the precipitation ones, from a few percent for ZIF-71 to up to 25% for ZIF-93. This could be due to the mesoporosity detected in both samples.

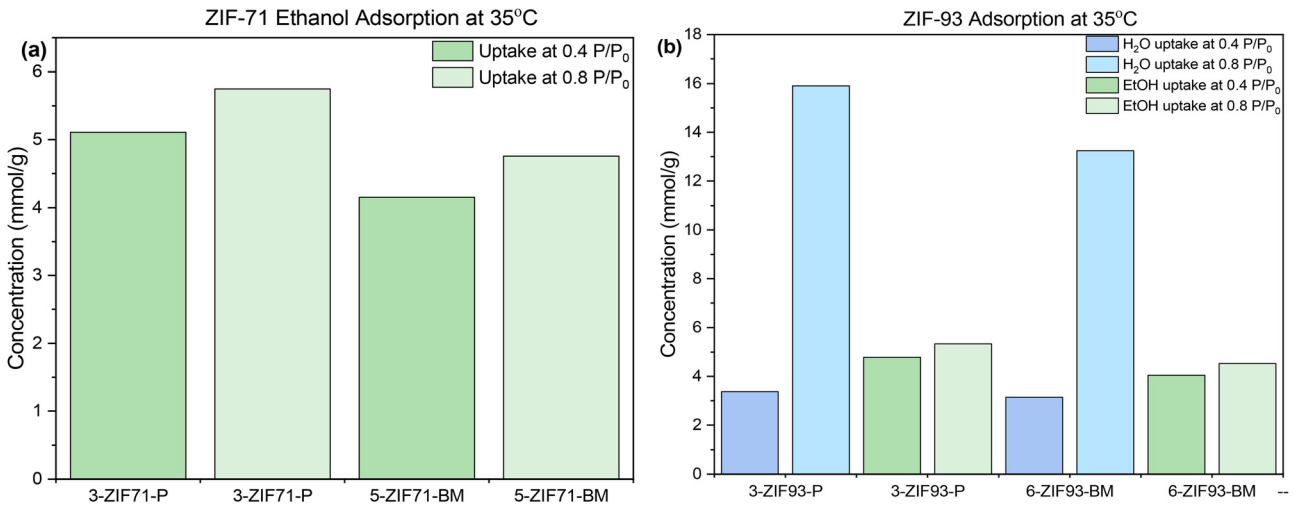

Fig. 9 Bar charts showing (a) ethanol uptake of ZIF-71, and (b) ethanol and water uptake of ZIF-93 obtained at 35 °C, with data for 0.4 P/P_0 and 0.8 P/P_0.

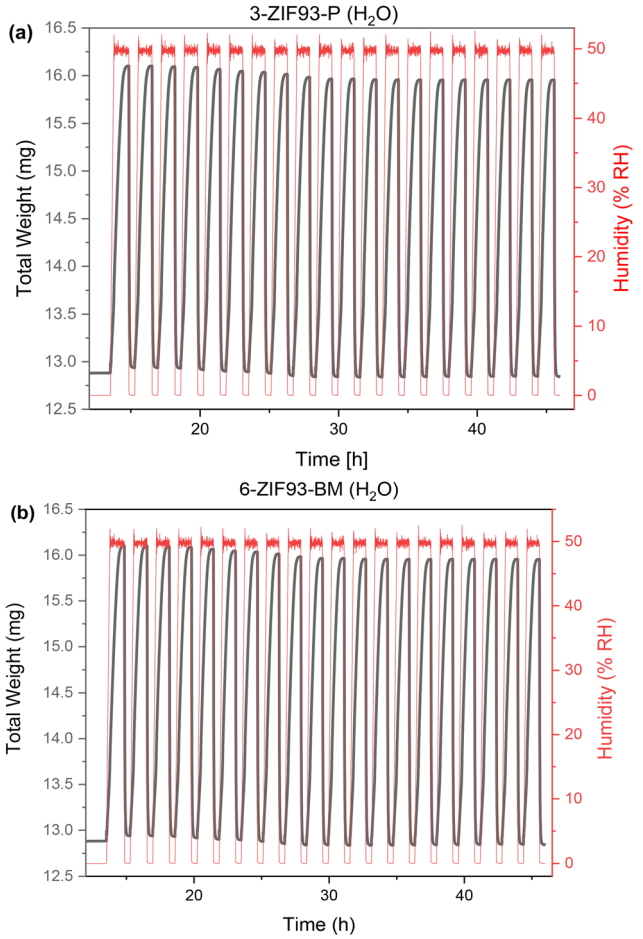

Fig. 10 Water cycling isotherms at 35 °C for (a) 3-ZIF93-P and (b) 6-ZIF93-BM.

Overall, both types of materials prepared by ball milling and precipitation maintain their initial capacity over the evaluated cycling program, suggesting their promising long-term performance, which is superior to the majority of MOF systems.[18,55] The sample stability was further confirmed by PXRD analysis of the used samples, revealing that the crystallinity was mostly preserved (Fig. 12).

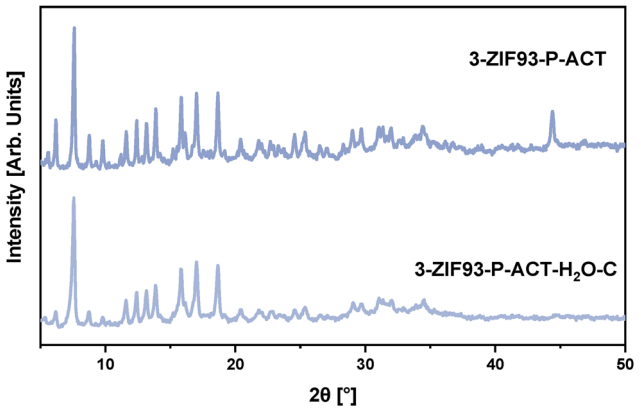

Fig. 12 PXRD of 3-ZIF93-P-ACT and the sample after water cycling at 35 °C.

Conclusions

In this study, ZIF-71 and ZIF-93 were synthesized using solvothermal, precipitation and mechanochemical methods. For the solvothermal synthesis, the methods from the literature were modified by changing different reaction parameters, such as the type of zinc precursor or solvent, reaction time and concentration of the reagents.

The precipitation method approach demonstrated the successful preparation of ZIF-93 samples at room temperature using water as a solvent, in 4 to 5 hours. Similar ethanol and water sorption capacities, higher porosity and higher specific surface area were achieved for these ZIF-93 samples in comparison to other samples synthesized solvothermally at 85 °C.

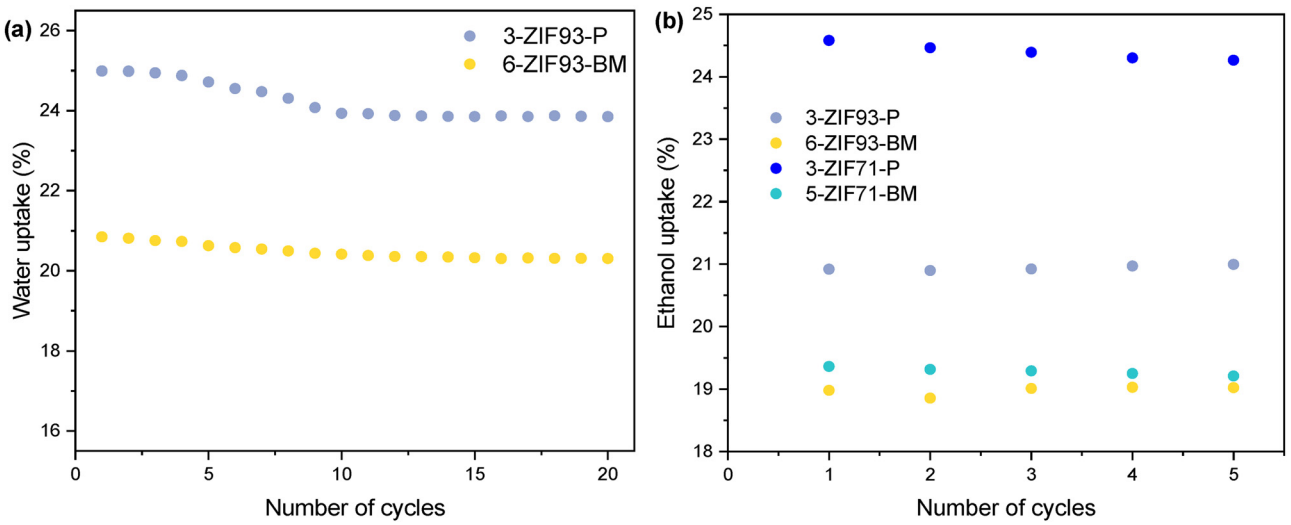

Fig. 11 The (a) % water and (b) % ethanol uptake for ZIF samples during cycling tests.

However, by changing the solvent used in the synthesis from methanol to ethanol and increasing the concentration of the reagents in the synthesis, the sorption performance of the ZIF-93 materials was reduced. For the ZIF-71 samples prepared by precipitation method, the adsorption capacities for ethanol, porosity and BET surface area are all decreased in comparison to the values for the solvothermal analogues. Water adsorption was negligible in all ZIF-71 samples.

The mechanochemical synthesis approach resulted in ZIF-93 and ZIF-71 products with reduced specific surface area and total pore volume, compared to the solvothermal samples. However, the water and ethanol uptake of the mechanochemical ZIF-93 sample was comparable to the uptake of the solvothermal samples. We can speculate that this could be due to the presence of SIM-1/ZIF-94 impurities that have higher reported water sorption capacity compared to ZIF-93, but its presence could not be confirmed. In the ZIF-71 system, the reduced ethanol capacity of ZIF-71 synthesized *via* liquid-assisted ball mill method might be due to a partial degradation of the structure during the adsorption studies. For that reason, further optimisations of the mechanochemical synthesis process is required for the ZIF-71 system.

The key result of this study is the proof of the relevant cycling stability of ZIF-93 and ZIF-71 prepared *via* both synthesis procedures (ball-milling and precipitation methods), and with the use of both adsorbates (water and ethanol). The study also revealed that water adsorption in the selected ZIFs is much faster than ethanol, which is a crucial parameter for sorption-based applications, like TCES and ACH.

Conflicts of interest

There are no conflicts to declare.

Data availability

The data supporting this article have been included as part of the ESI.†

Acknowledgements

This research was funded by the Slovenian Research Agency Research Program P1-0021, Research Program P1-0175 and Project J1-50020. The authors would like to thank Aljaž Škrjanc for assistance with the ball mill synthesis, Mojca Opresnik for SEM imaging and Edi Kranjc for PXRD measurements.

References

1 J. Li, P. M. Bhatt, J. Li, M. Eddaoudi and Y. Liu, *Adv. Mater.*, 2020, **32**, 1–18.
2 B. Fumey, R. Weber and L. Baldini, *Renewable Sustainable Energy Rev.*, 2019, **111**, 57–74.
3 R. Li and P. Wang, *Nat. Water*, 2023, **1**, 573–586.
4 A. Ristić, F. Fischer, A. Hauer and N. Zabukovec Logar, *J. Mater. Chem. A*, 2018, **6**, 11521–11530.
5 A. Ristić and N. Z. Logar, *Nanomaterials*, 2019, **9**(1), 27–42.
6 F. M. N. U. Khan, M. G. Rasul, A. S. M. Sayem and N. Mandal, *Energy Rep.*, 2023, **9**, 11–21.
7 H. Wu, F. Salles and J. Zajac, *Molecules*, 2019, **24**(5), 945.
8 S. K. Henninger, S. J. Ernst, L. Gordeeva, P. Bendix, D. Fröhlich, A. D. Grekova, L. Bonaccorsi, Y. Aristov and J. Jaenchen, *Renewable Energy*, 2017, **110**, 59–68.
9 A. Krajnc, J. Varlec, M. Mazaj, A. Ristić, N. Z. Logar and G. Mali, *Adv. Energy Mater.*, 2017, **7**, 1–8.
10 Y. Ban, Y. Peng, Y. Zhang, H. Jin, W. Jiao, A. Guo, P. Wang, Y. Li and W. Yang, *Microporous Mesoporous Mater.*, 2016, **219**, 190–198.
11 A. J. Brown, J. R. Johnson, M. E. Lydon, W. J. Koros, C. W. Jones and S. Nair, *Angew. Chem., Int. Ed.*, 2012, **51**, 10615–10618.
12 D. Chen, J. Zhao, P. Zhang and S. Dai, *Polyhedron*, 2019, **162**, 59–64.
13 C. Byrne, A. Ristić, S. Mal, M. Opresnik and N. Z. Logar, *Crystals*, 2021, **11**, 1422.
14 B. Chen, Z. Yang, Y. Zhu and Y. Xia, *J. Mater. Chem. A*, 2014, **2**, 16811–16831.
15 C. Byrne, M. Mazaj and N. Z. Logar, *Mater. Chem. Phys.*, 2025, **332**, 130143.
16 A. Ristić, N. Z. Logar, S. K. Henninger and V. Kaučič, *Adv. Funct. Mater.*, 2012, **22**, 1952–1957.
17 M. Gao, J. Wang, Z. Rong, Q. Shi and J. Dong, *RSC Adv.*, 2018, **8**, 39627–39634.
18 D. M. Steinert, S. J. Ernst, S. K. Henninger and C. Janiak, *Eur. J. Inorg. Chem.*, 2020, 4502–4515.
19 T. Johnson, M. M. Łozińska, A. F. Orsi, P. A. Wright, S. Hindocha and S. Poulston, *Green Chem.*, 2019, **21**, 5665–5670.
20 K. Zhang, R. P. Lively, M. E. Dose, A. J. Brown, C. Zhang, J. Chung, S. Nair, W. J. Koros and R. R. Chance, *Chem. Commun.*, 2013, **49**, 3245–3247.
21 M. F. De Lange, B. L. Van Velzen, C. P. Ottevanger, K. J. F. M. Verouden, L. C. Lin, T. J. H. Vlugt, J. Gascon and F. Kapteijn, *Langmuir*, 2015, **31**, 12783–12796.
22 M. Tu, C. Wiktor, C. Rösler and R. A. Fischer, *Chem. Commun.*, 2014, **50**, 13258–13260.
23 M. Shahsavari, P. M. Jahani, I. Sheikhshoaie, S. Tajik, A. A. Afshar, M. B. Askari, P. Salarizadeh, A. Di Bartolomeo and H. Beitollahi, *Materials*, 2022, **15**, 1–27.
24 H. Li, W. Chen, B. Liu, M. Yang, Z. Huang, C. Sun, C. Deng, D. Cao and G. Chen, *Green Energy Environ.*, 2023, **8**, 775–784.
25 A. Škrjanc, C. Byrne and N. Zabukovec Logar, *Molecules*, 2021, **26**(6), 1573.
26 L. Gong, Z. Cai, Q. Wu, L. Liu, C. Wang, L. Shan, X. Meng, S. Luo, Z. Liu and S. Zhang, *J. Mater. Chem. A*, 2022, **10**(47), 24975–24984.
27 R. Banerjee, A. Phan, B. Wang, C. Knobler, H. Furukawa, M. O'Keeffe and O. M. Yaghi, *Science*, 2008, **319**, 939–943.
28 H. Zhang, C. Duan, F. Li, X. Yan and H. Xi, *Inorg. Chim. Acta*, 2018, **482**, 358–363.

29 P. Cubillas, M. W. Anderson and M. P. Attfield, *Chem. – Eur. J.*, 2013, **19**, 8236–8243.
30 M. Gustafsson and X. Zou, *J. Porous Mater.*, 2013, **20**, 55–63.
31 Y. Li, L. H. Wee, J. A. Martens and I. F. J. Vankelecom, *J. Mater. Chem. A*, 2014, **2**, 10034–10040.
32 M. Yuan, Y. Zhao, W. Niu, Q. Shi, H. Xu, B. Zheng and J. Dong, *J. Mater. Eng. Perform.*, 2019, **28**, 1668–1677.
33 E. V. Ramos-Fernandez, A. Grau-Atienza, D. Farrusseng and S. Aguado, *J. Mater. Chem. A*, 2018, **6**, 5598–5602.
34 M. Švegovec, A. Škrjanc, A. Krajnc and N. Z. Logar, *Cryst. Growth Des.*, 2023, **23**, 3754–3760.
35 S. Kevat and V. N. Lad, *J. Organomet. Chem.*, 2023, **999**, 122832.
36 Y. N. Wu, J. Cai, S. Hou, R. Chen, Z. Wang, D. M. Kabtamu, O. A. Zelekew and F. Li, *Dalton Trans.*, 2024, **53**, 14098–14107.
37 C. R. Marshall, E. E. Timmel, S. A. Staudhammer and C. K. Brozek, *Chem. Sci.*, 2020, **11**, 11539–11547.
38 M. A. Molina, J. Rodríguez-Campa, R. Flores-Borrell, R. M. Blanco and M. Sánchez-Sánchez, *Nanomaterials*, 2024, **14**, 1–17.
39 C. R. Marshall, S. A. Staudhammer and C. K. Brozek, *Chem. Sci.*, 2019, **10**, 9396–9408.
40 R. S. Forgan, *Chem. Sci.*, 2020, **11**, 4546–4562.
41 C. A. Tao and J. F. Wang, *Crystals*, 2021, **11**, 1–20.
42 M. F. Thorne, M. L. R. Gómez, A. M. Bumstead, S. Li and T. D. Bennett, *Green Chem.*, 2020, **22**, 2505–2512.
43 R. Lin, Y. Yao, M. Y. Bin Zulkifli, X. Li, S. Gao, W. Huang, S. Smart, M. Lyu, L. Wang, V. Chen and J. Hou, *Nanoscale*, 2022, **14**, 2221–2229.
44 M. Taheri, T. G. Enge and T. Tsuzuki, *Mater. Today Chem.*, 2020, **16**, 100231.
45 W. Xu, H. Chen, K. Jie, Z. Yang, T. Li and S. Dai, *Angew. Chem., Int. Ed.*, 2019, **131**, 5072–5076.
46 J. Zhao, *Front. Mater.*, 2021, **8**, 1–7.
47 W. Morris, B. Leung, H. Furukawa, O. M. K. Yaghi, N. He, H. Hayashi, Y. Houndonougbo, M. Asta, B. B. Laird and O. M. K. Yaghi, *J. Am. Chem. Soc.*, 2010, **132**, 11006–11008.
48 A. Phan, C. J. Doonan, F. J. Uribe-romo, C. B. Knobler, M. O. Keeffe and O. M. Yaghi, *Acc. Chem. Res.*, 2010, **43**, 58–67.
49 W. Morris, C. J. Doonan, H. Furukawa, R. Banerjee and O. M. Yaghi, *J. Am. Chem. Soc.*, 2008, **130**, 12626–12627.
50 Y. Ding, H. Wang, M. Yu, W. Zheng, X. Ruan, X. Li, Y. Xi, Y. Dai, H. Liu and G. He, *Sep. Purif. Technol.*, 2023, **309**, 122949.
51 H. Zhang, K. Zhao, W. Guo, K. Liang, J. Li, X. Li, Q. Deng, X. Xu, H. Chao, H. Xi and C. Duan, *Ind. Chem. Mater.*, 2024, 109–121.
52 M. Wang, J. Wu, M. Gao, L. Ge, Q. Shi and J. Dong, *Sep. Purif. Technol.*, 2025, **352**, 128266.
53 S. Japip, H. Wang, Y. Xiao and T. S. Chung, *J. Memb. Sci.*, 2014, **467**, 162–174.
54 H. G. T. Nguyen, B. Toman, R. D. van Zee, C. Prinz, M. Thommes, R. Ahmad, D. Kiska, J. Salinger, I. M. Walton, K. S. Walton, D. P. Broom, M. J. Benham, H. Ansari, R. Pini, C. Petit, J. Adolphs, A. Schreiber, T. Shigeoka, Y. Konishi, K. Nakai, M. Henninger, T. Petrzik, C. Kececi, V. Martis, T. Paschke, E. Mangano and S. Brandani, *Adsorption*, 2023, **29**, 113–124.
55 T. B. Čelič, A. Škrjanc, J. M. Coronado, T. Čendak, V. A. de la Peña O'Shea, D. P. Serrano and N. Zabukovec Logar, *Nanomaterials*, 2022, **12**(12), 2092.